

Al_{0.68}Sc_{0.32}N/SiC based metal-ferroelectric-semiconductor capacitors operating up to 900 °C

Yunfei He¹, David C. Moore², Yubo Wang¹, Spencer Ware¹, Sizhe Ma¹, Dhiren K. Pradhan¹, Zekun Hu¹, Xingyu Du¹, W. Joshua Kennedy², Nicholas R. Glavin², Roy H. Olsson III¹ & Deep Jariwala¹

¹ Department of Electrical and System Engineering, University of Pennsylvania, Philadelphia, Pennsylvania 19104, USA

² Materials and Manufacturing Directorate, Air Force Research Laboratory, Wright-Patterson AFB, Dayton, OH, USA

Abstract:

Ferroelectric (FE)-based devices show great promise for non-volatile memory applications, yet few demonstrate reliable operation at elevated temperatures. In this work, we fabricated and characterized metal ferroelectric semiconductor capacitors integrating Aluminum Scandium Nitride onto Silicon Carbide, a prospective high temperature semiconductor for logic operations in extreme environments. The resultant Ni/Al_{0.68}Sc_{0.32}N/4H-SiC structure was evaluated for non-volatile memory performance from room temperature to high-temperature conditions. The 30-nm thick Al_{0.68}Sc_{0.32}N/SiC-based ferroelectric capacitors demonstrated ferroelectric switching at 900°C. The coercive field of the FE layer decreased linearly from $-6.4/+11.9$ MV cm⁻¹ at room temperature to $-3.1/+7.8$ MV cm⁻¹ at 800°C. Using positive-up negative-down measurements, we characterized the temperature dependence of remanent polarization. At 600°C, the devices achieved remarkable reliability, demonstrating endurance of ~2000 cycles and retention exceeding 100 hours with negligible polarization loss. Further reliability measurements extended to 800°C with 10,000 secs retention and > 300 endurance cycles, establish these devices as promising candidates for high-temperature memory applications.

1 Introduction

Nonvolatile memory (NVM) devices are critical for data storage across applications ranging from consumer electronics to industrial systems, where retaining information without power is essential. Various NVM technologies have been developed to meet these needs, including flash memory,¹ resistive random-access memory (RRAM),² magnetic random-access memory (MRAM),³ phase-change memory (PCM),⁴ and ferroelectric random-access memory (FeRAM). Among these competitors, ferroelectric-based memory devices have demonstrated superior characteristics, including fast programming time, low writing energy, and excellent endurance.⁵

Despite the growing need for NVM in high temperature applications, thermal stability remains a major obstacle for most NVM technologies, with commercially available products struggling to function reliably at temperatures exceeding 300 °C.⁶ While widely studied ferroelectric materials like hafnium zirconium oxide ($\text{Hf}_{1-x}\text{Zr}_x\text{O}$) show significant degradation such as — over 80% reduction in remanent polarization at 400 °C⁷, the wurtzite-structure III-nitride-based ferroelectric material aluminum scandium nitride ($\text{Al}_{1-x}\text{Sc}_x\text{N}$) is known for its large remnant polarization has emerged as a promising alternative⁸⁻¹¹ for NVM applications.^{12,13} With its high Curie temperature, AlScN has been reported to retain ferroelectricity after annealing at 1000 °C.¹⁴ Furthermore, in our former work, we have already demonstrated the high-temperature operation of the Ni/AlScN/Pt metal-insulator-metal (MIM) structure ferroelectric diode (FeD) NVM devices, showing long retention and high endurance at 600 °C.¹⁵

High-temperature digital circuits are crucial for aerospace, automotive, and energy exploration industries, where components must operate reliably in extreme thermal environments.¹⁶⁻¹⁹ Silicon carbide (SiC) is the model semiconductor material for high temperature electronics due to its high thermal stability and wide-band gap.²⁰ Thus, SiC-based devices have demonstrated functionality at temperatures up to 800 °C, while emphasizing the demands of a memory technology that is directly integrable with SiC.^{16,21-25} Building on the successful demonstration of Al/AlScN/SiC-based ferroelectric capacitors in our previous work,²⁶ we have now designed our devices for enhanced high-temperature performance. This study presents temperature-dependent measurements of Ni/ $\text{Al}_{0.68}\text{Sc}_{0.32}\text{N}$ /SiC metal-ferroelectric-semiconductor (MFeS) structure ferroelectric capacitors, specifically designed for compatibility with SiC-based integrated circuits, addressing the need for high-temperature digital circuits with embedded memory in extreme thermal environments.

2 Measurements and results

2.1 Fabrication and Electrical Characteristics of $\text{Al}_{0.68}\text{Sc}_{0.32}\text{N}/\text{SiC}$ Based Ferroelectric Capacitor under Room Temperature

A schematic of the $\text{Ni}/\text{Al}_{0.68}\text{Sc}_{0.32}\text{N}/\text{SiC}$ MFeS capacitor is shown in Figure 1(a). The fabrication process began with sputtering and patterning 200 nm-thick Ni onto a heavily n-type doped 4H-SiC wafer as bottom electrodes, followed by an annealing process to form Ohmic contacts between the Ni electrodes and SiC wafer. A 30 nm $\text{Al}_{0.68}\text{Sc}_{0.32}\text{N}$ ferroelectric layer was then co-sputtered directly onto the 4H-SiC wafer via methods previously reported.^{15,26} Subsequently, 200 nm-thick Ni top electrodes were sputtered using identical settings to the bottom electrodes and patterned by photolithography into circular pads with a diameter of ~ 60 μm . Atomic force microscopy (AFM) analysis of the 30-nm-thick $\text{Al}_{0.68}\text{Sc}_{0.32}\text{N}$ ferroelectric layer on SiC, shown in Figure 1(b), revealed a low surface roughness of 0.74 nm, indicating high-quality growth directly on the 4H-SiC wafer. Figure 1(c) presents a scanning electron microscopic (SEM) image of the patterned top Ni electrode pad, confirming an actual diameter of ~ 63 μm .

To characterize the coercive field and remanent polarization of the fabricated $\text{Ni}/\text{Al}_{0.68}\text{Sc}_{0.32}\text{N}/\text{SiC}$ ferroelectric capacitors, we employed two methods: bipolar fast sweep voltage for J-E hysteresis loop measurements and ultrafast pulsing using positive-up negative-down (PUND) measurement. Throughout this work, all measurements maintained a consistent configuration, applying voltage at the bottom electrodes while sensing the current response at the top electrodes. Figure 1(d) shows the J-E hysteresis loop obtained at room temperature under a bipolar triangular voltage sequence with a frequency of 10 kHz. An asymmetric voltage sequence was applied to compensate for the voltage drop across the depletion region of the heavily n-type doped SiC substrate, with significantly higher positive voltage compared to the negative direction.²² The J-E hysteresis loop revealed current density peaks indicating ferroelectric switching under both positive and negative applied voltages. The coercive field (E_c) was estimated at -6.4 MV cm^{-1} and $+11.9 \text{ MV cm}^{-1}$ at 10 kHz, consistent with our previous work.^{11,14,22} However, substantial leakage current under positive voltage prevented accurate determination of the current density peaks from the ferroelectric contribution and reliable

estimation of the remanent polarization (Pr). Therefore, we implemented PUND measurements to determine the remanent polarization.

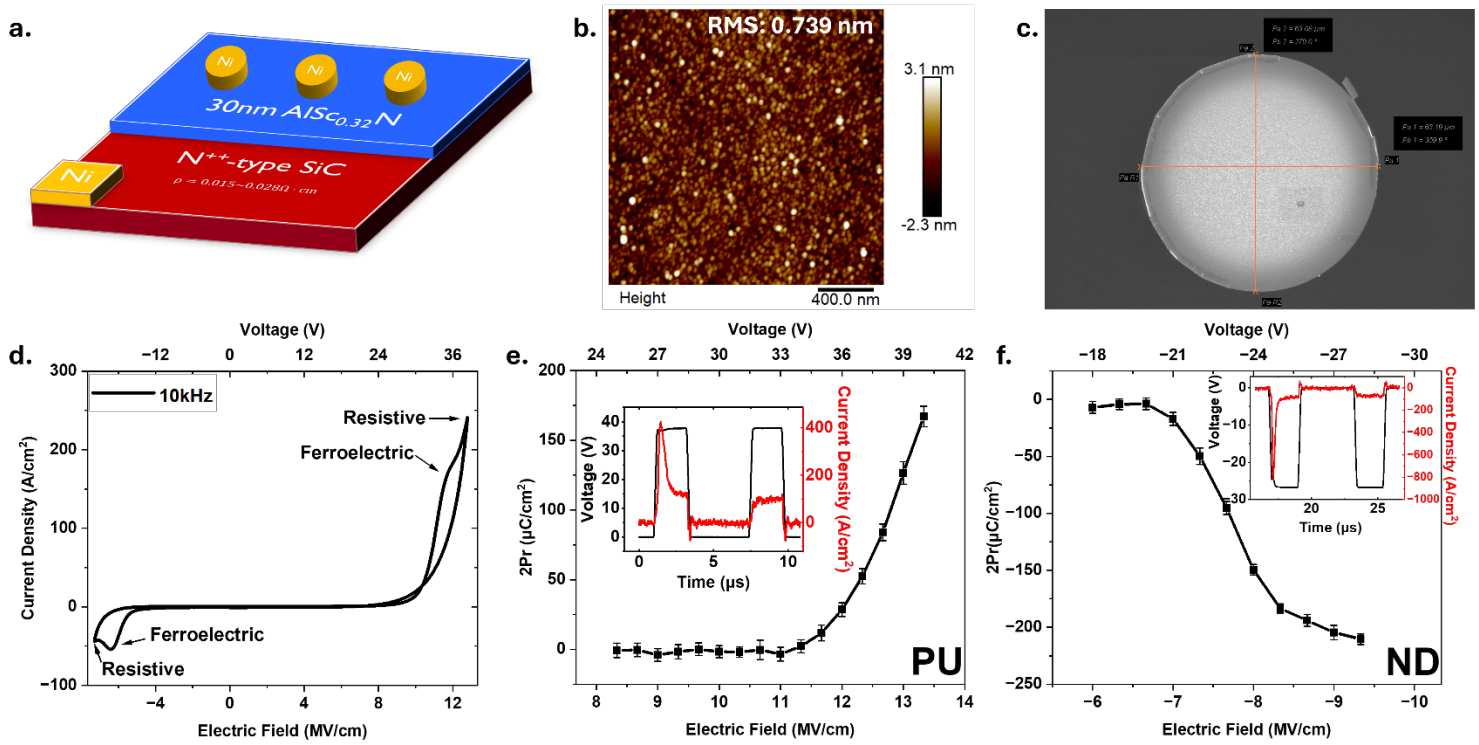


Fig. 1. (a) Schematic of the Ni/Al_{0.68}Sc_{0.32}N (30nm)/4H-SiC metal-ferroelectric-semiconductor (MFeS) capacitor.

Both top and bottom electrodes are sputtered Ni with a thickness of 200 nm. **(b)** AFM of the surface topology of the 30-nm-thick Al_{0.68}Sc_{0.32}N ferroelectric film directly growth on the 4H-SiC wafer, exhibiting a low surface roughness of 0.74 nm. **(c)** SEM image of the top Ni electrode pad of the fabricated device, with an actual diameter of 63.1 μm. **(d)** J-E hysteresis curve of the demonstrated MFeS capacitor at 10 kHz, the black arrows indicate the current density peaks due to leakage current and ferroelectric switching current components, respectively. **(e)** and **(f)** The remanent polarization ($2P_r$) calculated from PUND measurement on ten (10) Al_{0.68}Sc_{0.32}N/SiC ferroelectric capacitors under different voltage applied in both **(e)** negative and **(f)** positive directions. The $2P_r$ are normalized by the area of the top electrodes, and the error bar indicates the device-to-device variation of the fabricated capacitors. The inset displays the current response to the PU pulse sequence and the ND pulse sequence, respectively. The current density peaks indicate ferroelectric switching.

The remanent polarization ($2P_r$) calculated from PUND measurements across ten (10) Al_{0.68}Sc_{0.32}N/SiC ferroelectric capacitors at varying pulse voltages at room temperature are shown in Figure 1(e) and (f). The insets show transient current responses with corresponding voltage pulses for "PU" and "ND" sequences. For all pulse sequences ("P", "U", "N", and "D"), we employed a rise/fall time of 100 ns and pulse width of 2 μs. Polarization values were obtained by integrating the current response over time for each sequence, followed by subtracting the "U" and "D" pulse sequence polarizations from the "P" and "N" sequences to estimate $2P_r$ in both voltage directions. Results showed a saturated Pr of $-105.2 \pm$

$2.3 \mu\text{C cm}^{-2}$ for the "ND" sequences at 28 V, matching our previous findings.²² For "PU" sequences, the large uncompensated leakage current due to asymmetric voltage application resulted in continuously increasing 2Pr with positive voltage. We further developed a modified measurement approach using a triangular voltage sequence with two positive and two negative voltage segments. By subtracting the second positive/negative segment's current response from the first, we obtained clearer current density curves relative to applied electric field, revealing more distinct ferroelectric-related current density peaks in both voltage directions [See Supplementary Information S3].

2.2 Electrical Characteristics of $\text{Al}_{0.68}\text{Sc}_{0.32}\text{N}/\text{SiC}$ Based Ferroelectric Capacitor at Elevated Temperature

We investigated the high-temperature performance of the fabricated $\text{Al}_{0.68}\text{Sc}_{0.32}\text{N}/\text{SiC}$ ferroelectric capacitors through J-E hysteresis and PUND (positive-up negative-down) measurements across temperatures ranging from room temperature to 900°C. All experiments were conducted under vacuum conditions at pressures below 5.7 mTorr. Figure 2(a) presents the J-E hysteresis curves measured at 10 kHz for selected temperatures. As temperature increased, we observed a dramatic rise in leakage current, necessitating a reduction in applied voltage to prevent device breakdown at elevated temperatures. Despite this voltage adjustment, ferroelectric switching current density peaks remained observable. At 900°C, the leakage current in the positive direction reached 10 mA, corresponding to the current compliance limit of the measurement tool (indicated by the black dashed line in Figure 2(a)). Notably, in the negative direction, a distinct current density peak attributable to ferroelectric switching remained observable at 900°C. The temperature dependence of the coercive field (E_C) was extracted from the J-E curves and is presented in Figure 2(b). The E_C exhibited a linear decrease from $-6.4/+11.9 \text{ MV cm}^{-1}$ at RT to $-3.1/+7.8 \text{ MV cm}^{-1}$ at 800 °C. The E_C further reduces to $\sim -2 \text{ MV cm}^{-1}$ at 900 °C, demonstrating a continued reduction in coercive field with increasing temperature. Figure 2(c) illustrates the current response from PUND measurements at selected temperatures. To ensure consistency in obtaining saturated remanent polarization at different temperatures, we started from low voltages for the PUND sequences and progressively increased them at each temperature until the calculated remanent polarization reached saturation. This approach allowed us to accurately capture the remanent polarization

while preventing the increased leakage current from breaking down the devices at high temperatures. [See Supplementary information S4].

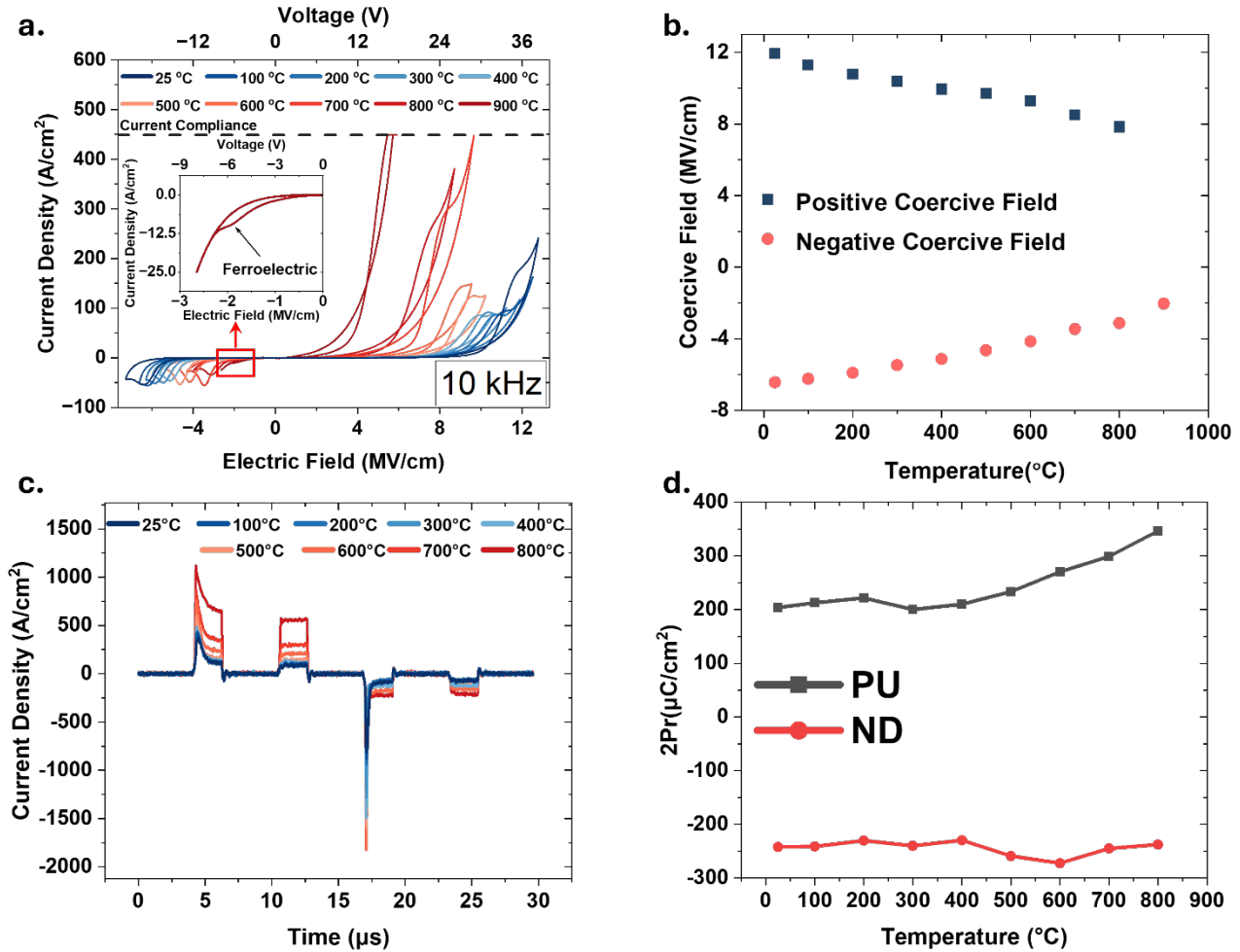


Fig. 2. (a) 10 kHz J-E hysteresis loops of the fabricated Al_{0.68}Sc_{0.32}N/SiC ferroelectric capacitor at elevated temperatures (T) with a range from RT (25 °C) to 900 °C. The applied voltage decreases when increasing the temperature, to accommodate the rising leakage current and to prevent the device from breaking down. The black dashed line indicates the measured current compliance of the tool. Inset: a magnified region that highlights the ferroelectric switching of the demonstrated device at 900 °C. (b) Coercive field (E_C) calculated from the J-E hysteresis loop with respect to the measured temperature. (c) Current response of a single asymmetric PUND measurement on the ferroelectric capacitor under elevated temperatures. (d) Saturated remanent polarization ($2P_r$) calculated from the current response of the PUND measurements. Note that the $2P_r$ for PU pulse sequence above 600 °C is not conclusive due to the uncompensated leakage current.

Figure 2(d) presents the saturated remanent polarization ($2P_r$) calculated by integrating the current response from the PUND measurements. The remanent polarization in ND sequences remains relatively stable, with the P_r of $-118.7 \mu\text{C cm}^{-2}$ at 800 °C. On the other hand, the remanent polarization in PU sequences starts rising drastically at 600 °C since the uncompensated leakage current increases with temperature in the positive directions. At

500 °C and lower temperatures, the remanent polarization P_r maintains at approximately $+116.8 \mu\text{C cm}^{-2}$, showing consistency with the results obtained from the ND sequences and aligning with our previous work at room temperature.²¹ Due to equipment limitations, the chamber pressure in the high-temperature probe station increased [See Supplementary Information Table S2 for chamber pressure with respect to the temperatures]. This pressure increase likely led to oxidation of the top electrodes, preventing us from obtaining reliable PUND measurements at 900°C and above.

2.3 Reliability of $\text{Al}_{0.68}\text{Sc}_{0.32}\text{N}/\text{SiC}$ Based Ferroelectric Capacitors at Elevated Temperature

Through J-E hysteresis curves and PUND measurements, we demonstrated that the $\text{Al}_{0.68}\text{Sc}_{0.32}\text{N}$ film maintains stable ferroelectric characteristics at temperatures up to 900°C. This thermal stability establishes $\text{Al}_{0.68}\text{Sc}_{0.32}\text{N}/\text{SiC}$ -based devices as promising candidates for memory applications in high-temperature circuit designs. Given that reliability is crucial for memory devices, particularly in elevated temperature operations, we conducted comprehensive investigations of retention and endurance characteristics at high temperatures, with specific focus on performance at 600 °C.

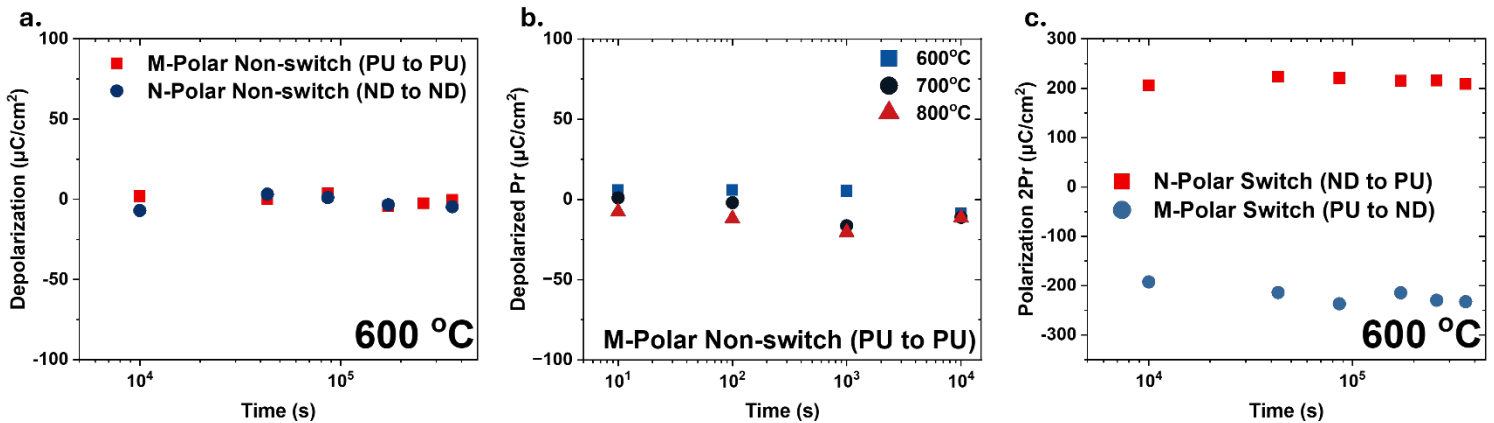


Fig. 3. (a) Same state retention performance on the demonstrated $\text{Al}_{0.68}\text{Sc}_{0.32}\text{N}/\text{SiC}$ -based capacitor in both Metal-Polar (M-Polar) and Nitrogen-Polar (N-Polar) directions at 600 °C. (b) Same state retention performance in M-Polar direction of the ferroelectric capacitor at selected elevated temperatures. (c) Opposite state retention performance in both M-Polar and N-Polar directions at 600 °C.

To evaluate the retention performance of the $\text{Al}_{0.68}\text{Sc}_{0.32}\text{N}/\text{SiC}$ -based capacitors, we conducted both same state and opposite state retention tests based on PUND pulse measurements with different pulse sequence configurations while maintaining the devices at high temperature. [See Supplementary information S5 for details of the non-switching and switching retention pulse sequences.] By integrating the current response from the pulsed voltage sequences, we calculated the amount of depolarized polarization from same state retention measurements and $2P_r$ from switching methods. Figure 3(a) presents an ultra-low depolarization in both Metal-Polar (PU sequence followed by another PU sequence) and Nitrogen-Polar (ND sequence

followed by another ND sequence) after 3.6×10^5 s (100 hours) at 600 °C, with a polarization loss of $-0.4/-4.7 \mu\text{C cm}^{-1}$ in M-Polar and N-Polar after 100 hours, respectively. Note that the negative depolarization in the M-Polar is mainly due to the leakage current and cycle-to-cycle variation of the demonstrated ferroelectric capacitor. In the N-Polar direction, the polarization depolarized by only 3.4% of its remanent polarization at 600 °C, which demonstrates significant retention at the selected temperature. Since the demonstrated $\text{Al}_{0.68}\text{Sc}_{0.32}\text{N}$ ferroelectric thin film was co-sputtered on SiC with an initial polarization direction of N-Polar, it is more susceptible for the ferroelectric film to be depolarized when programmed in the M-Polar direction. Therefore, we concentrated our retention analysis on the ferroelectric capacitor in the M-Polar state at higher temperatures up to 800 °C. Figure 3(b) shows the same state retention results of the $\text{Al}_{0.68}\text{Sc}_{0.32}\text{N}/\text{SiC}$ -based capacitors programmed in the M-Polar direction at selected temperatures with a retention time ranging from 10^1 s to 10^4 s. Over 10^4 s, the ferroelectric film retained its polarization in the M-Polar direction with no significant depolarization at the selected temperatures. It is important to note that at 700 °C and 800 °C, increased leakage current and the cycle-to-cycle variation had a greater impact on the calculated depolarization, resulting in further negative depolarization in the M-Polar direction. Since the same state retention measurement in the M-Polar direction yielded negative depolarization value, which was inconclusive, we proceeded with opposite state retention measurements on the ferroelectric capacitor at 600 °C. These measurements were carried out concurrently on six (6) separate devices, each set with different retention times, with the longest retention time of 3.6×10^5 s (100 hours), as shown in Figure 3(c). The remanent polarization $2P_r$ remained stable, with values of $-116.2/+104.3 \mu\text{C cm}^{-2}$ at 3.6×10^5 s, compared to $-96.3/+102.8 \mu\text{C cm}^{-2}$ at 10^4 s. This indicates no significant depolarization in either the M-Polar or N-Polar directions, demonstrating excellent retention stability over extended periods at high temperatures.

We continued to evaluate the endurance of the $\text{Al}_{0.68}\text{Sc}_{0.32}\text{N}/\text{SiC}$ -based ferroelectric capacitor as another aspect of the high temperature reliability of the ferroelectric film. Figure 4(a) presents the endurance cycles based on PUND measurement at selected temperatures, ranging from room temperature (25 °C) to 800 °C. To measure the endurance of the fabricated ferroelectric capacitors, we employed a single-positive-single-negative fatigue pulse sequence, with preset iteration cycles between each PUND measurement, where the $2P_r$ was measured. For each fatigue pulse sequence, the same voltage used in the PUND measurement was applied at each temperature. Prior to each endurance measurement at each temperature, multiple PUND measurements with incrementally increasing voltages were conducted, similar to the method described in Supplementary Information 4, to achieve saturated polarization. Once the voltage corresponding to saturated polarization at the selected temperature was determined, it was applied for five PUND pulses as wake-up cycle, then applied for both fatigue and PUND pulses to measure the endurance of the fabricated devices. This approach minimized the risk of device breakdown from uncompensated leakage current and ensured effective ferroelectric

switching. At RT (25 °C), the measured device endured 4.9×10^3 cycles under $-24/+38$ V fatigue pulses with a pulse width of 2 μ s, demonstrating improved endurance compared to our previous works. As temperature increases, the endurance cycling decreases, with endurance of 369 cycles under $-15/+23$ V at 800 °C. At 600 °C, the demonstrated devices reliably switched for up to 1.9×10^3 cycles before breaking down, highlighting its relatively strong endurance at elevated temperatures. We also conducted endurance measurements on five devices that were maintained at 600 °C for over 100 hours, with the applied voltage of $-15/+31$ V, displayed in Figure 4(b). Note that these measurements were performed while the devices remained at 600 °C, and the devices can endure up to 2×10^3 cycles at most. Both retention and endurance tests at high temperatures demonstrate the high reliability of the $\text{Al}_{0.68}\text{Sc}_{0.32}\text{N}/\text{SiC}$ -based ferroelectric capacitors, positioning AlScN/SiC-based ferroelectric devices as strong contenders for high-temperature memory device applications.

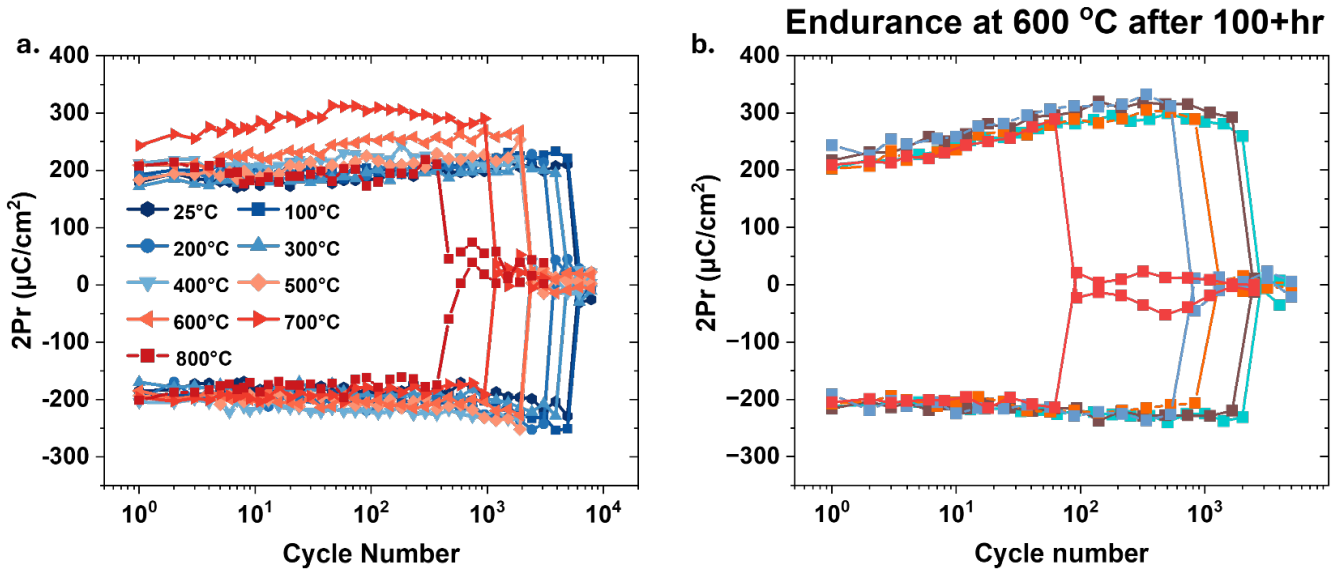


Fig. 4. (a) Calculated $2P_r$ of the demonstrated $\text{Al}_{0.68}\text{Sc}_{0.32}\text{N}/\text{SiC}$ -based capacitors, based on PUND measurement, is shown with respect to the number of fatigue pulses at selected temperatures, ranging from RT to 800 °C. (b) Calculated $2P_r$ for five ferroelectric capacitors at 600 °C, with the sample maintained at 600 °C for over 100 hours.

3 Conclusion

In this study, high-temperature operation of $\text{Al}_{0.68}\text{Sc}_{0.32}\text{N}/\text{SiC}$ -based metal ferroelectric semiconductor capacitors was demonstrated. Through J-E hysteresis and PUND measurements, the temperature-dependent properties were evaluated, including coercive field (E_C) and remanent polarization (P_r), from room temperature up to 800 °C, with partial E_C measurements extending to 900 °C. The devices exhibited exceptional high-temperature reliability in both retention and endurance tests. At 600 °C, the capacitors maintained stable remanent

polarization for 3.6×10^5 s (100 hours) with negligible depolarization and sustained 2000 cycles after 100 hours of heating at 600 °C. Even at 800 °C, the devices demonstrated retention exceeding 10,000 s and endurance of 369 cycles. These results establish AlScN/SiC-based ferroelectric capacitors as promising candidates for high-temperature memory applications. Their compatibility with SiC-based logic devices addresses a critical gap in high-temperature integrated circuits, offering a reliable memory solution for extreme thermal environments.

4 Experimental Section

4.1 Al_{0.68}Sc_{0.32}N Ferroelectric Thin Film Preparation

Thin film of 30 nm Al_{0.68}Sc_{0.32}N was grown directly on the 350 μm thick heavily n-type doped 4H-SiC (Powerway Wafer Co., Limited, Nitrogen N-type Doped, resistivity of $\rho = 0.015\text{--}0.028 \Omega \cdot \text{cm}$) with a co-sputtering system (Evatec Clusterline 200 II) at 350 °C, with a N₂ gas flow of 30 sccm. The Al target and Sc target sputtering powers were set as 1000 W and 655 W, respectively, to create 32% Sc concentration.

4.2 Device Fabrication

Before the ferroelectric thin film was deposited, a 200-nm-thick Ni bottom electrodes was first sputtered (Lesker PVD75 DC/RF Sputterer) and patterned on the corner of the 4H-SiC wafer, following an annealing process at 1050 °C for 2 min with Argon flow to form the ohmic contact between the metal and semiconductor interface. After the deposition of the AlScN ferroelectric thin film, 200-nm-thick Ni top electrodes were patterned using a lift-off process and Ni deposition under the same settings described above.

4.3 Device Characterizations

All electrical characteristics measurements, including J-E hysteresis, PUND, retention and endurance tests, were performed by a Keithley 4200A-SCS parameter analyzer, with built-in nonvolatile memory (NVM) library. The tested samples were placed in a vacuum chamber probe station (HP1000V-MPS, Instec Inc), with a heated stage providing selected temperature environments for temperature-dependent measurements. In the J-E hysteresis measurements, we applied a bipolar triangular wave with a frequency of 10 kHz to obtain temperature-dependent coercive field. For the PUND and reliability measurements, each single pulse in the pulse sequences was a voltage pulse with a rise/fall time of 200 ns and a pulse width of 2 μs, using temperature-dependent voltages to measure and calculate the remanent polarization and reliability of the fabricated ferroelectric capacitors.

5 Acknowledgement

D.J., R.H.O. and Y.H. acknowledge primary support for this work from AFRL via the FAST program D.J. also acknowledges support from the Air Force Office of Scientific Research (AFOSR) GHz-THz program FA9550-23-1-0391. N.R.G. and D.C.M. gratefully acknowledge

support from Air Force Office of Scientific Research (AFOSR) GHz-THz program grant number FA9550-24RYCOR011.

6 Author Contributions

D.J., R.H.O., Y.H. conceived the concepts of devices, measurements and sample fabrications; Y.H. and Z.H fabricated the samples with assistance from X.D.; the device is measured at RT with assistance from D.K.P., S.M.; Y.H., D.C.M., S.M., Y.W., and S.W. performed all the high temperature measurements; Y.H., D.C.M., and Y.W. analyzed all the electrical data; Y.H. performed AFM measurement; D.C.M. performed SEM measurement; All data analysis are under supervision of D.J., R.H.O.; N.R.G. and W.J.K. guided the project. Y.H. wrote the manuscript. All authors provided their inputs to the paper and Supplementary Information.

References

1. Zhao, Chun, et al. "Review on non-volatile memory with high-k dielectrics: Flash for generation beyond 32 nm." *Materials* 7.7 (2014): 5117-5145.
2. Gupta, Varshita, et al. "Resistive random access memory: a review of device challenges." *IETE Technical Review* 37.4 (2020): 377-390.
3. Sousa, Ricardo C., and I. Lucian Prejbeanu. "Non-volatile magnetic random access memories (MRAM)." *Comptes Rendus Physique* 6.9 (2005): 1013-1021.
4. Ismail, Kamal AR, et al. "A Comprehensive Review on Phase Change Materials and Applications in Buildings and Components." *ASME Open Journal of Engineering* 1 (2022).
5. Kim, Kwan-Ho, et al. "Wurtzite and fluorite ferroelectric materials for electronic memory." *Nature Nanotechnology* 18.5 (2023): 422-441.
6. Memory products for high temperature, harsh environments. *TTSemiconductor* (accessed 30 September 2023). <https://ttsemiconductor.com/Memory-Products-For-High-Temperature-Harsh-Environments-1003-295.html>
7. Azevedo Antunes, Luis, et al. "Insights Into Curie-Temperature and Phase Formation of Ferroelectric $\text{Hf}_{1-x}\text{Zr}_x\text{O}_2$ with Oxygen Defects from a Leveled Energy Landscape." *Advanced Materials Interfaces* 11.2 (2024): 2300710.
8. Wang, Dixiong, et al. "Ferroelectric switching in sub-20 nm aluminum scandium nitride thin films." *IEEE Electron Device Letters* 41.12 (2020): 1774-1777.
9. Liu, Xiwen, et al. "Aluminum scandium nitride-based metal-ferroelectric-metal diode memory devices with high on/off ratios." *Applied Physics Letters* 118.20 (2021).
10. Wang, Dixiong, et al. "Sub-microsecond polarization switching in (Al, Sc) N ferroelectric capacitors grown on complementary metal-oxide-semiconductor-compatible aluminum electrodes." *physica status solidi (RRL)-Rapid Research Letters* 15.5 (2021): 2000575.

11. Zheng, Jeffrey X., et al. "Ferroelectric behavior of sputter deposited Al_{0.72}Sc_{0.28}N₂ approaching 5 nm thickness." *Applied Physics Letters* 122.22 (2023).
12. Liu, Xiwen, et al. "Reconfigurable compute-in-memory on field-programmable ferroelectric diodes." *Nano letters* 22.18 (2022): 7690-7698.
13. Kim, Kwan-Ho, et al. "Scalable CMOS back-end-of-line-compatible AlScN/two-dimensional channel ferroelectric field-effect transistors." *Nature nanotechnology* 18.9 (2023): 1044-1050.
14. Islam, Md Redwanul, et al. "On the exceptional temperature stability of ferroelectric Al_{1-x}Sc_xN thin films." *Applied Physics Letters* 118.23 (2021).
15. Pradhan, Dhiren K., et al. "A scalable ferroelectric non-volatile memory operating at 600° C." *Nature Electronics* (2024): 1-8.
16. Neudeck, Philip G., et al. "Demonstration of 4H-SiC digital integrated circuits above 800° C." *IEEE Electron Device Letters* 38.8 (2017): 1082-1085.
17. Thompson, H. A. "Application of commercial off-the-shelf technologies to aerospace gas turbine engine control." (1997): 2-2.
18. Balint, Tibor S., et al. "Extreme environment technologies for space and terrestrial applications." *Space Exploration Technologies*. Vol. 6960. SPIE, 2008.
19. Werner, Matthias Ralf, and Wolfgang R. Fahrner. "Review on materials, microsensors, systems and devices for high-temperature and harsh-environment applications." *IEEE Transactions on Industrial Electronics* 48.2 (2001): 249-257.
20. Pradhan, Dhiren K., et al. "Materials for high-temperature digital electronics." *Nature Reviews Materials* (2024): 1-18.
21. Neudeck, Philip G., et al. "Extreme temperature 6H-SiC JFET integrated circuit technology." *physica status solidi (a)* 206.10 (2009): 2329-2345.
22. Spry, David, et al. "Experimental durability testing of 4H SiC JFET integrated circuit technology at 727 C." *Micro-and Nanotechnology Sensors, Systems, and Applications VIII*. Vol. 9836. SPIE, 2016.
23. Kimoto, T., et al. "An Overview of SiC High-Voltage Power Devices and High-Temperature ICs." *2024 IEEE BiCMOS and Compound Semiconductor Integrated Circuits and Technology Symposium (BCICTS)*. IEEE, 2024.
24. Monaghan, Finn, et al. "A 4H-SiC JFET with a monolithically integrated temperature sensor." *Power Electronic Devices and Components* 8 (2024): 100069.
25. Neudeck, Philip G., et al. "Upscaling of 500° C Durable SiC JFET-R Integrated Circuits." *Additional Papers and Presentations 2021.HiTEC* (2021): 000064-000068.
26. He, Yunfei, et al. "Metal-ferroelectric AlScN-semiconductor memory devices on SiC wafers." *Applied Physics Letters* 123.12 (2023).

Supplementary Material

$\text{Al}_{0.68}\text{Sc}_{0.32}\text{N}/\text{SiC}$ based metal-ferroelectric-semiconductor capacitors operating up to $900\text{ }^{\circ}\text{C}$

Yunfei He¹, David C. Moore², Yubo Wang¹, Spencer Ware¹, Sizhe Ma¹, Dhiren K. Pradhan¹, Zekun Hu¹, Xingyu Du¹, W. Joshua Kennedy², Nicholas R. Glavin², Roy H. Olsson III¹ & Deep Jariwala¹

¹ Department of Electrical and System Engineering, University of Pennsylvania, Philadelphia, Pennsylvania 19104, USA

² Materials and Manufacturing Directorate, Air Force Research Laboratory, Wright-Patterson AFB, Dayton, OH, USA

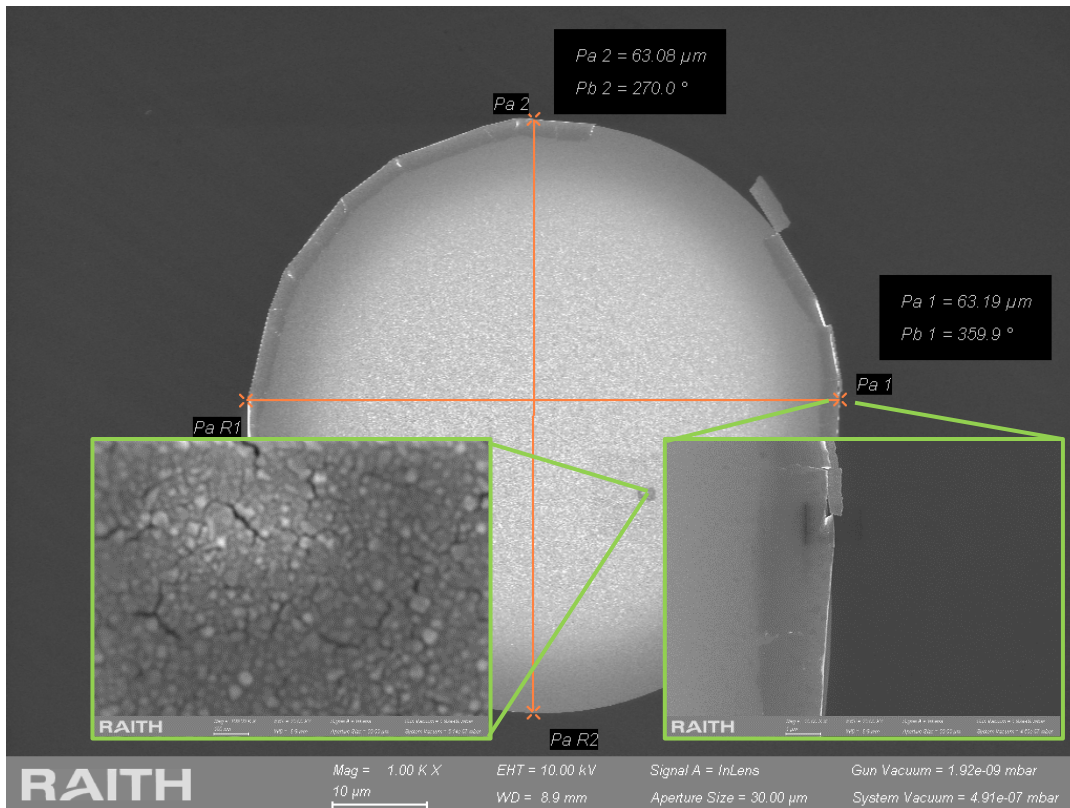


Figure S1. Scanning electron microscopy (SEM) image showing the patterned Ni top electrode pad post high T measurements, with the actual diameter of $63.1\text{ }\mu\text{m}$. The left inset presents a zoomed-in view of the region where the probe was applied. The right inset displays a close-up of the edge of the Ni top electrode, revealing cracks, which are assumed to have been caused by high temperature treatment during the measurements.

Temperature (°C)	Chamber pressure (mTorr)
100	3.4
200	3.4
300	3.5
400	3.8
500	4.3
600	4.7
700	5.2
800	5.7
900	7.8

Table S2. The temperature-dependent chamber pressure of the probe station shows an increase in pressure as temperature increases. This pressure increase is primarily attributed to the limitations of the vacuum conditions within the probe station chamber.

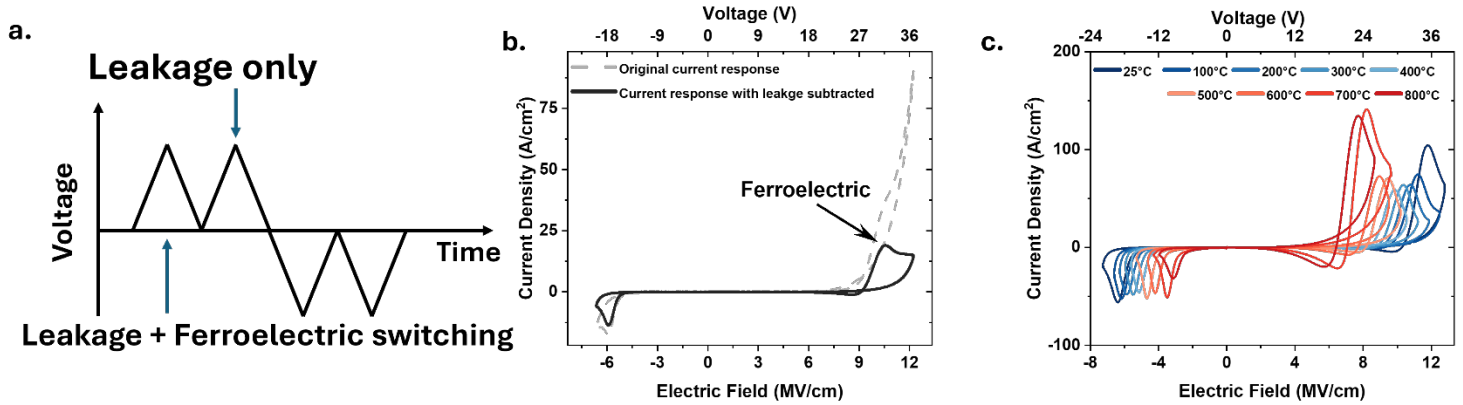


Figure S3. (a) A schematic of the wave sequences consists of two positive triangular pulses and two negative triangular pulses, each with a rise/fall time of 25 μ s. In the first positive and first negative triangular waves, the current response is expected to include both leakage and ferroelectric switching. In contrast, the second positive and second negative triangular waves are anticipated to show a current response that is primarily due to leakage current. (b) a comparison between the original current density response obtained from AC J-E measurement in Figure 2 of the manuscript (dashed black data) and the results with the leakage compensated (solid black data). The leakage compensated results were derived by subtracting the current density response of the second positive/negative triangular waves from the first positive/negative triangular waves. This mathematical approach clarifies the current density peak associated with ferroelectric switching, making it more observable. (c) the temperature-dependent current density response was measured at selected temperatures, ranging from RT (25 °C) to 800 °C using the aforementioned leakage compensation method. The current density peaks contributed by ferroelectric switching are clearly observed in both voltage directions at each selected temperature. Note that the negative current density response between 0 MV cm⁻¹ and 8 MV cm⁻¹ at high temperatures is a result of pure mathematical subtraction. This occurs due to the increased carrier mobility at the Al_{0.68}Sc_{0.32}N/SiC interface, which enhances the leakage current under the second positive pulse, leading to a negative result from the subtraction.

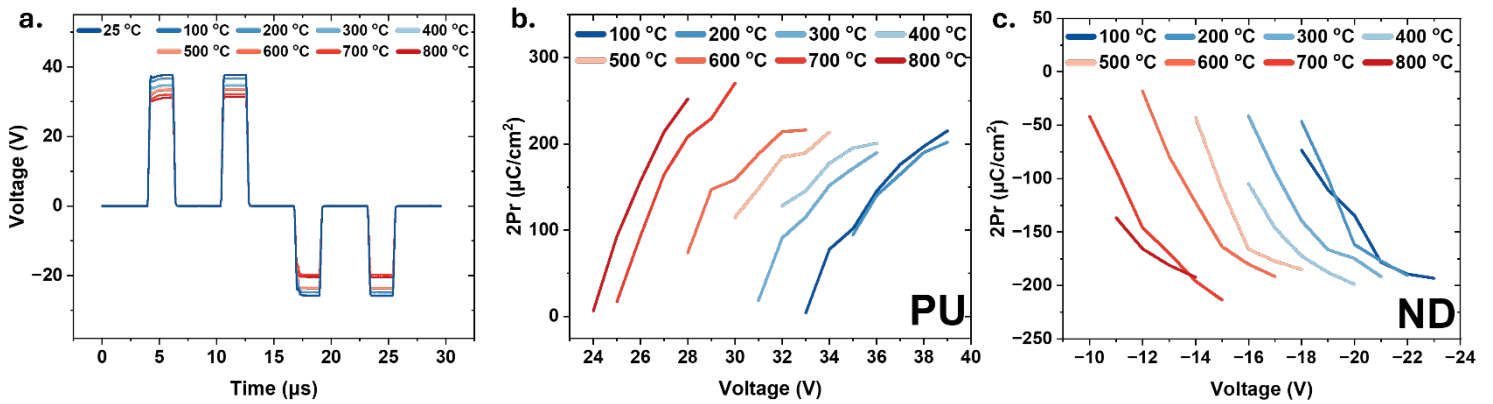


Figure S4. (a) The PUND measurement voltage sequences at selected temperatures are presented, corresponding to the current response in Figure 2(c), showing a clear trend of decreasing applied voltage as temperature increases. This adjustment is necessary to prevent the device from breaking down by the thermal-induced leakage current. (b) and (c) display the remanent polarization ($2P_r$) as a function of the applied voltage in the PUND measurement in (b) positive and (c) negative directions, respectively. Note that the $2P_r$ in the positive direction (corresponding to PU sequences) increases drastically due to the thermal-induced leakage current. In contrast, a saturation polarization at each selected temperature is clearly observed in the negative direction (ND sequences), indicating stable ferroelectric switching despite the temperature changes.

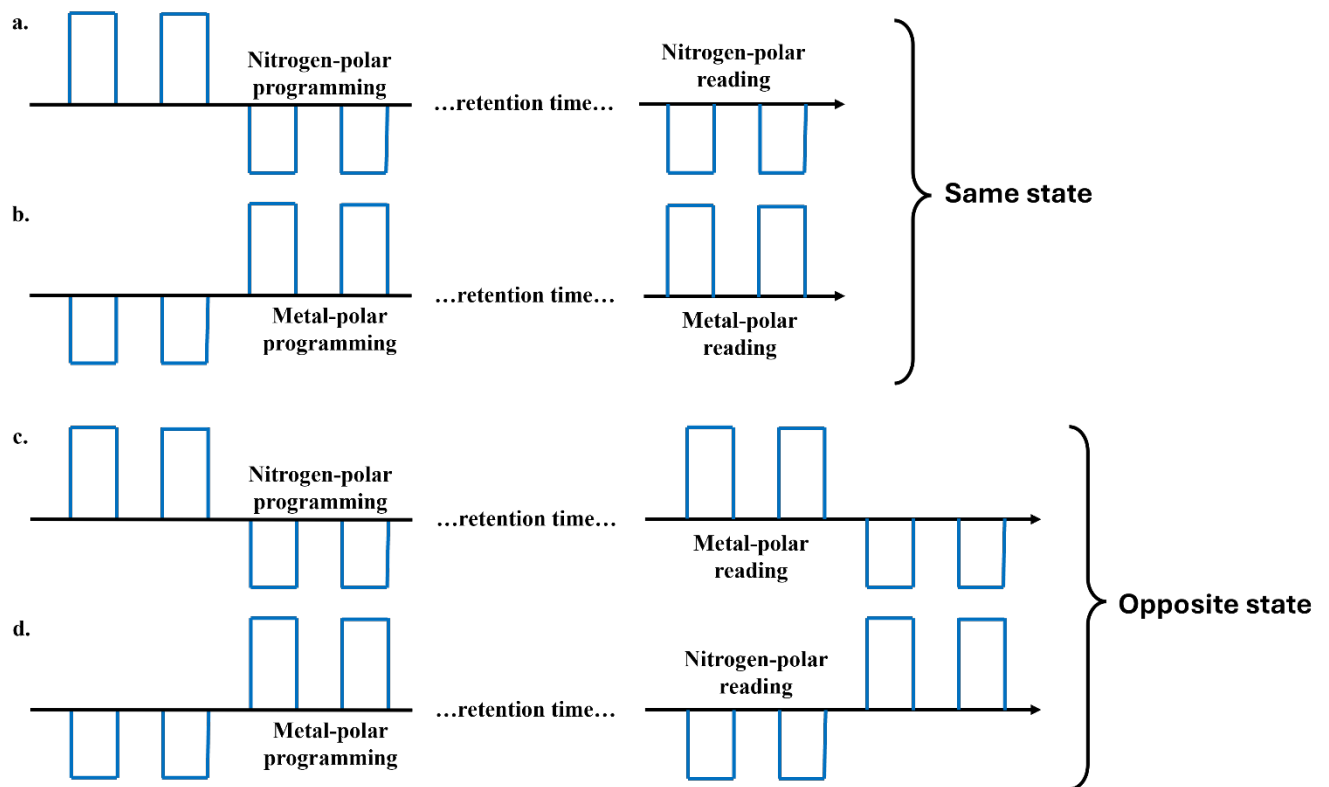


Figure S5. The (a-b) same state and (c-d) opposite state retention measurement pulse sequence schematic using PUND ultra-fast pulsing measurements.^{1,2} For same state retention measurements, we first applied a (a) PUND ((b)NDPU) four pulse sequence to programming the device fully in the Nitrogen-polar (Metal-polar). Then after a certain retention time, we applied a ND (PU) sequence again to obtain the same state non-switched polarization, as the amount of polarization loss. For opposite state retention measurements, we obtained the polarization corresponding to (c) N-polar/ (d) M-polar after different sets of retention times. Each “P”, “U”, “N”, and “D” pulse sequence applied has a pulse width of 2 μ s, rise/fall time of 200 ns, and pulse delay of 4 μ s.

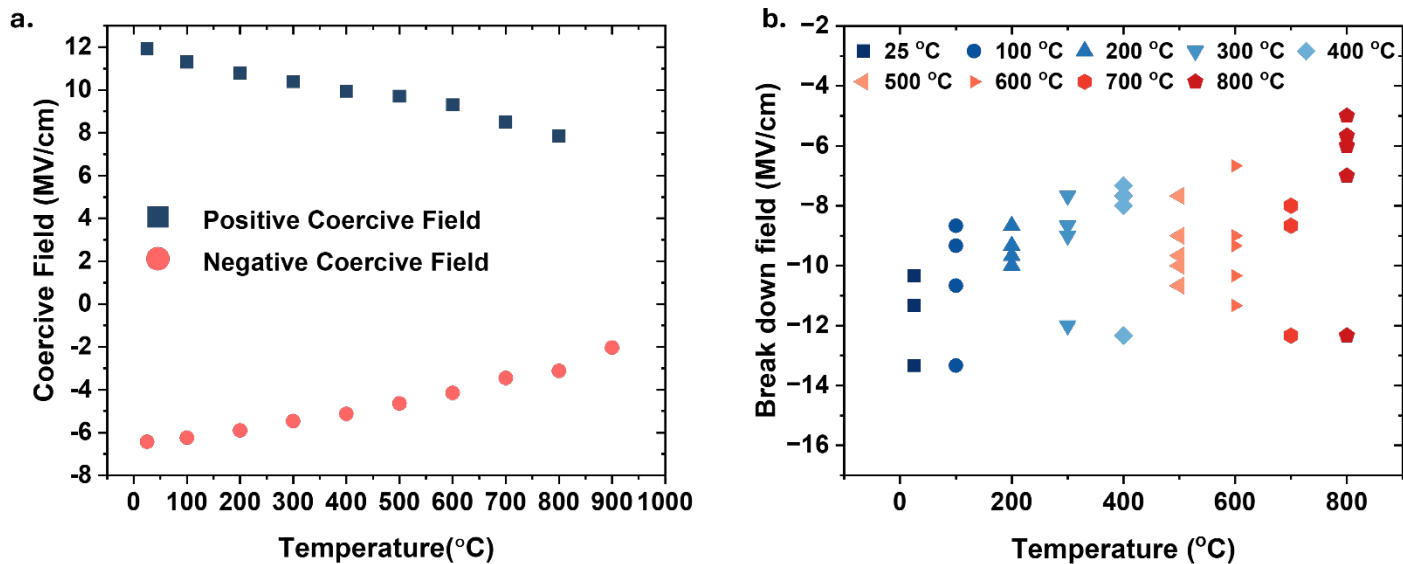


Figure S6. (a) Coercive field (E_C) calculated from the J-E hysteresis loop with respect to the measured temperature. (b) Break down field (E_{BD}) of five devices at each selected temperature in the negative voltage directions based on J-E hysteresis loop measurements. A trend of the absolute value of the break down field decreasing with rising temperature is observed.

Reference

1. Zhu, Wanlin, et al. "Exceptional high temperature retention in Al_{0.93}B_{0.07}N films." *Applied Physics Letters* 122.24 (2023).
2. He, Yunfei, et al. "Metal-ferroelectric AlScN-semiconductor memory devices on SiC wafers." *Applied Physics Letters* 123.12 (2023).